Investigation of three-dimensional wind flow behaviour over coastal dune morphology under offshore winds using computational fluid dynamics (CFD) and ultrasonic anemometry

D. W. T. Jackson[1], J. H. M. Beyers[2], K. Lynch[3], J. A. G. Cooper[1], A. C. W. Baas[4], and I. Delgado-Fernandez[1]

[1]Centre for Coastal & Marine Research, School of Environmental Sciences, University of Ulster, Coleraine, Co. Londonderry, UK
[2]Rowan Williams Davies and Irwin, Guelph, Ontario, Canada
[3]Department of Geography, National University of Ireland, Galway, Ireland
[4]Department of Geography, King's College London, Strand, London WC2R 2LS, UK

ABSTRACT

The behaviour of offshore-directed winds over coastal dune and beach morphology was examined using a combination of modelling (3-D computational fluid dynamics (CFD)) and field measurement. Both model simulations and field measurements showed reversal of offshore flows at the back beach and creation of an onshore sediment transport potential. The influence of flow reversals on the beach-dune transport system and foredune growth patterns has previously received little attention. Detailed wind flow measurements were made using an extensive array of mast-mounted, 3-D ultrasonic anemometers (50 Hz), arranged parallel to the dominant incident wind direction. Large eddy simulation (LES) of the offshore wind flow over the dune was conducted using the open-source CFD tool openFOAM. The computational domain included a terrain model obtained by airborne LiDAR and

detailed ground DGPS measurements. The computational grid (~22 million cells) included localized mesh refinement near the complex foredune terrain to capture finer details of the dune morphology that might affect wind flows on the adjacent beach.

Measured and simulated wind flow are presented and discussed. The CFD simulations offer new insights into the flow mechanics associated with offshore winds and how the terrain steering of wind flow impacts on the geomorphological behaviour of the dune system. Simulation of 3-D wind flows over complex terrain such as dune systems, presents a valuable new tool for geomorphological research, as it enables new insights into the relationship between the wind field and the underlying topography. The results show that offshore and obliquely offshore winds result in flow reversal and onshore directed winds at distances of up to 20 m from the embryo dune toe. The potential geomorphological significance of the findings are discussed and simple calculations show that incoming offshore and obliquely offshore winds with mean velocities over 13 m s^{-1} and 7 m s^{-1}, respectively, have the potential to create onshore-directed winds at the back beach with mean velocities above 3.3 m s^{-1}. These are above the threshold of movement for dry sand and support previous conclusions about the significance of offshore winds in dune and beach budget calculations.

Keywords:

airflow; coastal foredunes; CFD; aeolian sediment transport; lee-side coasts

Introduction

A principal component of sediment budget analysis in the beach and foredune environment is the identification of wind events capable of aeolian sediment transport from the beach to the adjacent coastal dune field (Anthony *et al.*, 2007; Delgado-Fernandez and Davidson-Arnott, 2010). Sediment budget calculations routinely exclude offshore wind (Fryberger, 1979; Illenberger and Rust, 1988) because the cosine effect implies no sediment input into the dunes for winds approaching at an angle larger than ±90° from onshore perpendicular (Bauer and Davidson-Arnott, 2003). Localized sheltering by foredunes was also thought to lower offshore winds speeds on the back beach and to create sub-threshold conditions for sediment movement regardless of the incoming wind magnitude (Gares *et al.*, 1993). The existence of extensive aeolian dunes on coasts where the dominant wind direction is offshore (leeside coasts) is therefore difficult to explain within the traditional assumptions of foredune morphodynamics and regional shifts in wind regime are often invoked to explain their evolution (Shennan and Andrews, 2000). Numerous studies reporting on complex interactions between the wind field and underlying topography, and the resulting topographic steering of the wind have contributed to a change in this view. Hesp (2005), for example, suggested that topographic steering of the wind field resulting in a flow reversal, was the dominant mechanism in the development of climbing dunes on a leeside coast in New Zealand. Research in deserts (Frank and Kocurek 1996a, b; Baddock *et al.*, 2007) and wind tunnels (Walker and Nickling, 2003) indicates that airflow across dunes results in a wide range of turbulent processes at the lee side, such as flow separation and reattachment, deflected flow and reversed eddies, or complex roller vortices or roller helixes (Walker and Nickling, 2002). Spatio-temporal variability of

shear stress within turbulent flows helps maintain entrainment of grains (Baas and Sherman, 2005). Hence, flow velocities below the threshold for dry sand do not necessarily result in cessation of sediment transport providing turbulent conditions prevail (Wiggs *et al.*, 1996). The existence of a range of processes resulting in conditions favourable for transport toward the foredune suggests that the effects of offshore winds should be included in sediment budget calculations.

For this to happen, the dynamics of airflow and sand transport under offshore winds need to be better understood. The investigation of flow and transport dynamics under offshore wind regimes, however, is hampered by fundamental limitations in technology and methodologies. Recently, however, field experiments (Lynch *et al.*, 2008, 2009, 2010) measured (rather than simply inferred) landward aeolian sediment transport associated with local topographic steering of offshore directed airflow and established the basis to understand the importance of offshore flows on lee-side coasts. Lynch *et al.* (2009, 2010) showed that post-storm recovery of wave-scarped foredunes relied almost exclusively on offshore winds; flow reversals from these winds transported sand from the beach onto the scarped section and thus aided reconstruction of a dune ramp. The role of offshore wind events was such that their omission from sediment budget calculations resulted in large under-estimation of predicted sediment input to the foredune in the long-term (Lynch *et al.*, 2008). However, the degree of steering and magnitude of the reversed flow varied depending on wind direction and foredune morphology (Lynch *et al.*, 2010) which could explain why reversed flows have been considered inconsequential in sediment transport dynamics on other coastlines (Nordstrom *et al.*, 1996; Nordstrom *et al.*, 2006; Walker *et al.*, 2006). It is therefore important to explore the conditions under which offshore winds play a major role in coastal dune dynamics. This

99 requires the adoption of methodologies that are able to resolve turbulence in a 3-
100 dimensional environment, where changes in wind direction and terrain morphology
101 can be considered.
102 Computational fluid dynamics (CFD) models have been applied widely to a number
103 of natural settings using both 2-dimensional (Jackson and Hunt, 1975; Castro, 1991;
104 Byrne and Holdo, 1998; Abe *et al.*, 1993; Nicholas, 2001; Safarzadeh *et al.*, 2009)
105 and more recently 3-dimensional numerical simulations (Lane *et al.*, 2002; Nguyen
106 and Nestmann, 2004; Inkratas, *et al.*, 2009; Shi and Huang, 2010). In particular the
107 3-D modelling approach can provide detailed patterns of flow behaviour over non-
108 uniform topography (Lee *et al.*2002; Lun *et al.*, 2003; Stangroom, 2004), enabling a
109 more thorough examination of complex environments such as natural dune forms
110 and their associated airflow fields. Attempts to apply 2-D CFD to the investigation of
111 aeolian dunes have been promising. Parsons *et al.* (2002) validated a 2-D numerical
112 model based on PHOENICS™ 3.5 code using experimental wind tunnel flow
113 measurements obtained by Walker and Nickling (2003). Measured and predicted
114 velocities agreed in general but significant disagreement was found in the lower
115 velocities at the lee separation zone. A 2-D model was used by Parsons *et al.* (2004)
116 to simulate wind flow over a single idealized transverse dune of different dimensions
117 to explore processes such as relations between dune size and re-attachment points.
118 More recently, Wakes *et al.*(2010) successfully compared 2-D numerical simulations
119 against field data collected with cup anemometers and a wind vane at a coastal dune
120 complex at Manson Bay, New Zealand, showing the potential of CFD tools to
121 improve modelling of flows over complex surfaces.
122 Advances in the application of 3-D simulations of wind flow over coastal dunes are
123 desirable for a number of reasons. CFD allows a much more complete spatial

coverage of the wind field to be assessed than could be achieved from an instrumental approach. Simulations could be used to investigate the role of offshore winds under a wide range of scenarios. The detailed output resolution of the CFD models can also be used to inform field instrument deployments for optimal data gathering. Progress in this area to date has been limited by computing power, a lack of cross-disciplinary collaboration and the operational challenges of collecting the appropriate types of data at suitable spatial and temporal resolution for calibration of CFD simulations. Finally, there is a need to better characterize the wind field in key areas such as the lee separation zone.

This paper reports results of a project that aims to measure and model wind flow and aeolian sediment transport under offshore winds at a beach-dune system on a lee-side coast. The results from a deployment of an array of 3-D sonic anemometers across the beach–dune interface and associated 3-D CFD simulations using a detailed 3-D topographic surface model are presented. Model simulations were compared with field data to obtain a first assessment of the performance of the model at different heights over a given dune profile. Full validation of the 3-D model simulations will be discussed in future articles but examples are presented here to highlight the potential of CFD as a tool in the study of coastal dunes. The aim of this paper therefore is to investigate the existence of significant secondary airflows and the potential of CFD tools to model them correctly. The objectives are (1) to assess whether the onshore-directed flow under both perpendicular and oblique offshore winds is *transport-capable*; (2) to evaluate the performance of a number of turbulence models and explore the effect of introducing roughness into the simulations; (3) to discuss the potential of 3-D airflow simulations to provide insights into important feedbacks between form (dune shape/size) and processes (wind flow).

149 The first part of the paper describes field and modelling methods and results. The
150 second part compares field data with model simulations. The final section discusses
151 geomorphological implications of the work and future research, such as
152 measurements of sediment transport at the beach and temporal changes in
153 topography.
154
155 **Site Location**
156 The field experiment took place at Magilligan Strand, Northern Ireland, where a
157 range of foredune topographies exist. The strand is part of a 6 km-long, north-west to
158 south-east sandy beach system (Jackson *et al.*, 2005) extending from Magilligan
159 Point to Benone Strand (Figure 1). The wind regime is dominated by (offshore)
160 south-westerly winds (see insert in Figure 1). The foredune is largely linear and
161 unbroken and approximates an idealised transverse ridge. Previous research has
162 shown that the foredunes are of sufficient height (up to 11 m) to induce significant
163 secondary airflow effects (Lynch *et al.*, 2008, 2010). Dune vegetation consists of a
164 dense, homogenous cover of marram grass (*Ammophila arenaria*) with an average
165 height of 0.35 m. The adjacent beach is planar and generally unvegetated with little
166 surface debris. Beach and dune sediments consist of uniform, well-sorted, fine-
167 grained quartz sand (mean diameter 0.17 mm). The experimental site falls within a
168 military area which provided security for the instruments. An established regional
169 meteorological station providing continuous records of wind speed and direction is
170 located at Malin Head, 30 km north-west of the site.
171
172 **Methods**
173

Field data

Twenty-four ultrasonic anemometers (3-D Gill HS-50 model), were configured into a series of six vertical arrays (masts) to capture vertical and horizontal components of the wind over the foredune and across the beach surface (Figure 2). Sensor height locations (1 to 16.3 m above the local beach/dune surface) were based on a preliminary CFD run. The rig line was positioned in a near perpendicular orientation to the coastline. Each sensor had a measurement elevation angle of +/−50° from the horizontal and *u* (horizontal streamwise), *v* (horizontal spanwise), *w* (vertical) wind components were sampled at 50 Hz. Data were transferred to the serial communications from the ultrasonic anemometers (UAs) directly back to the control station position where they were time-stamped and buffered before transfer to a desktop PC. The wind speed accuracy of the windsonics is <1% RMS and the wind speed resolution is 0.0 1 ms^{-1}. The directional accuracy is < ± 1° RMS and the directional resolution is 1°.

Monitoring offshore winds covered a period of 11 days, from 23 September to 4 October 2009, and resulted in a total of 137 h with a diversity of wind speeds and directions. This extensive high quality data set contains rich information about turbulence, streamline patterns, and other wind characteristics that are explored in future publications. Only those processing steps leading to variables needed for CFD comparison purposes (magnitude of wind velocity and direction) are explained here. Wind direction (the angle in the horizontal plane between the incoming wind vector and the geographical north) was first calculated by rotating the coordinate system such that the *u*component of the wind aligned with the geographical north and thus misalignments due to orientations of UAs in the field were corrected. The angle between *u* and *v* was then calculated using the *atan2* function. Note that in field

199 situations where wind direction is highly variable the *atan2* is preferable to
200 the *arctangent* function, which only returns arguments in the half-plane (i.e. if
201 both *u* and *v* are negative,*arctangent* will give an angle measurement less than 90°,
202 while the angle should be between 180° and 270°). The magnitude of wind velocity
203 was calculated by considering the three components of the wind field (*u, v, w*) and
204 thus this includes horizontal and vertical accelerations. This paper does not deal with
205 streamline curvature (angle between the horizontal plane and *w*) or any of the
206 corrections associated with it (Walker, 2005; van Boxel *et al.*, 2004) as no Reynolds
207 stresses or quadrant analysis (burst-sweep cycles) are presented.
208 Synchronized 10 min averaging records of wind velocity and direction were obtained
209 at each of the sensors, representing a total of 822 runs. Runs were binned according
210 to wind direction at the reference sensor (6 m height in mast 1 – Figure 2) which
211 represented the incoming wind direction both for the field data and the CFD
212 simulations. Wind direction and velocity varied widely during measurement periods
213 but only those runs in which wind direction at the reference sensor matched two
214 particular wind directions (cases) were selected for the purpose of this paper. Walker
215 and Nickling (2003) suggested that offshore incident wind angles above 70° relative
216 to dune ridge direction resulted in flow separation while angles from 10–70° resulted
217 in attached and deflected flows. Case 1 contained perpendicular offshore winds
218 (90 ± 5° relative to dune ridge direction) and resulted in a total of 29 runs. Case 2
219 contained oblique offshore winds (53 ± 5° relative to dune ridge direction) and
220 resulted in a total of 35 runs. These corresponded with winds from 217° and 270°
221 with respect to geographical north (Figure 3) and represent 8% of the total data
222 collected. Finally, the average velocity at all sensors was normalized by the average

223 velocity at the reference sensor to obtain a velocity ratio (*vr*) that could be compared
224 with the CFD modelling results.
225
226 *Computational fluid dynamics simulations*
227 Topographic survey
228 A LiDAR survey of the entire Magilligan foreland was completed in June 2008 using
229 a LADS MKII LiDAR producing surface terrain data corrected to Belfast Lough
230 Datum using observed tides at Green Castle and Londonderry Port. The spatial
231 resolution of the spot data was every 4 m using the spheroid ETRF89 and projection
232 UTM, zone 29N, CM 9°W. A section of coastline measuring approximately 150 m
233 (longshore) × 250 m (cross-shore) was then isolated as the area of interest within
234 which the instrument rig was deployed (see detail on Figure 1). To supplement
235 topographic LiDAR mapping, a detailed DGPS survey of the beach and foredune
236 crest consisting of more than 48 000 points was also undertaken during September
237 to October 2009 using a Trimble 4800 RTK at a point sampling resolution of
238 1 m × 1 m. This was necessary to measure any topographic changes that may have
239 occurred in the foredune and beach area from sea wave and aeolian activity since
240 the original LiDAR survey. In addition, DGPS data points were gathered along the
241 main frontal foredune ridge crest at a resolution of 0.2 m × 0.2 m to examine
242 topographic detail on the crestal region. For compatibility all data from the DGPS
243 surveys were translated into UTM zone 29 and merged with the LiDAR data to
244 complete a detailed topographic mesh surface (Figure 3). The importance of
245 including the detailed DGPS survey data was highlighted in early investigative CFD
246 work applied to the LiDAR generated terrain only. The lower spatial resolution
247 provided by the LiDAR data at the dune crest, unrealistically smoothed the modelled

terrain crest, which reduced or eliminated the onset of a foredune recirculation zone in the simulations.

Computational fluid dynamics (CFD) methods

Previous CFD studies of wind flows over complex terrain have been performed to evaluate the performance of different modelling strategies, especially the ability of turbulence models to predict the measured behaviour of the accelerating and separating flow in three dimensional terrains. Most notable is the CFD validation work carried out for comprehensive wind measurements at Askervein hill (Salmon*et al.*, 1988) and the earlier comparative computational work performed by Raithby *et al.* (1987). Using a RNG (renormalization group technique) k–ε turbulence model at Askervein hill, Kim and Patel (2000) observed that predicted and measured mean wind speed and turbulence kinetic energy agreed well at the windward acceleration zone but disagreed in the leeward recirculation zone. This was confirmed by Castro *et al.* (2003) using the standard k–ε turbulence model, who attributed the discrepancies between measured and simulated results for the leeward flow regions to the non-constant surface roughness, the limitations of the turbulence model to deal with the anisotropic nature of the turbulence and streamline curvature and transient nature of the flow. Predictions of the leeward flow anisotropic turbulence characteristics at Askervein hill were improved later by Bechmann and Sorensen (2010) using hybrid RANS (Reynolds averaged Navier Stokes)/LES (large eddy simulations) simulations. LES can resolve turbulence characteristics far away from terrain surfaces but requires too many grid points near the wall to resolve the near wall turbulence structures. RANS simulation law-of-the-wall turbulence modelling strategies offer a compromise by modelling the near wall turbulence rather than

explicitly resolving the flow scales. A combination of both schemes can reduce computational grid counts and are typically classed as hybrid RANS/LES or alternatively as detached eddy simulation (DES) models with a variety of schemes to determine when to switch from LES to RANS schemes in the solution domain. A more comprehensive overview of the development of the hybrid methods and variations to the theme is given by Spalart (2009) and Fröhlich and Terzi (2008). Spalart and Allmaras (1994) originally developed a one-equation RANS model (SA-RANS) that solves a single transport equation for the eddy viscosity, described in Fröhlich and Terzi (2008). The SA-RANS eddy viscosity transport equation contains a turbulence destruction term that is a function of the wall distance (d). In the subsequent DES approach developed by Spalart *et al.* (1997), the wall distance was replaced by a length scale dependent on the grid size (Δ) which modifies the SA-RANS model into a LES SGS model. In this SA-DES model the length scale switches between wall distance (RANS) and grid size (LES). The grid length scale used in this model is the maximum of the three dimensional grid spacing instead of the more traditional cube root of the grid volume. One of the disadvantages of earlier DES models was its sensitivity to grid induced separation (GIS) where well-intentioned grid refinement approaches may actually reduce the accuracy of an LES simulation and can produce less accurate results than traditional RANS simulations on coarser grids (Spalart, 2009). One of the strategies to reduce the GIS effect resulted in the delayed DES (DDES) (Spalart *et al.*, 2006), which extends the RANS region by detecting boundary layers, rather than the LES/RANS switching over simply being controlled as a function of the wall distance or grid size alone. The improved delayed detached eddy simulation (IDDES) of Shur *et al.* (2008) is a further derivative of the DDES which combines the DDES with wall-modelling LES

298 (WMLES) and blends the applied RANS and LES length scales. For details on
299 modified length scales formula and blending functions see Fröhlich and Terzi (2008)
300 and Shur *et al.* (2008).
301 Simulations were carried out using the open-source CFD software OpenFOAM to
302 solve the system of partial differential equations representing the governing fluid
303 dynamic equations on a three-dimensional computational grid using finite volume
304 discretization strategies. The general flow solver follows standard CFD solution
305 techniques of finite volume discretization and pressure–velocity coupling techniques
306 (Shur *et al.*, 2008). The present work evaluated four turbulence modelling
307 approaches: (1) steady state RANS formulation using the RANSk–ω SST (shear
308 stress transport) turbulence model of Menter (1994); (2) the IDDES model of Shur *et*
309 *al.* (2008); (3) the one equation eddy (k) LES; and (4) an approach using the one
310 equation eddy (k) LES-ABL (atmospheric boundary layer) simulations that accounted
311 for terrain roughness by including a constant aerodynamic roughness length (z_0) in a
312 law of the wall logarithmic velocity profile that updates the near wall-eddy viscosity
313 (see Boundary conditions section). While a number of assumptions needed to be
314 considered, the aim of the fourth approach was to evaluate the impact of including
315 roughness into the simulations rather than discussing an appropriate method for
316 calculating z_0.
317
318 Boundary conditions
319 As in previous studies (Wakes *et al.*, 2010) several simplifications were adopted for
320 the purpose of conducting the simulations. The approaching wind profile was judged
321 to be similar to flow over open natural terrain. A logarithmic wind velocity profile was

used to provide the steady wind speed variation over the height of the domain inlet and also applied as the law of the wall function for the LES-ABL simulations:

$$U(z) = \frac{u_*}{\kappa} \ln\left(\frac{z + z_0}{z_0}\right) \quad (1)$$

where $U(z)$ is the wind speed at elevation z and K is the von Karman's constant (≈0.4). The aerodynamic surface roughness length (z_0) and shear velocity (u_*) for all simulations was 0.1 m and 0.70 m s^{-1}, respectively, and were estimated from mean wind profiles at masts 1–3 (over the dune field) using the method proposed by Namikas *et al.* (2003). The inlet turbulent kinetic energy (k), specific turbulence dissipation rate (ε), eddy viscosity and turbulence intensity profiles used for the simulations were derived from the turbulence inlet conditions given by Richards and Hoxey (1993):

$$k = \frac{u_*^2}{\sqrt{C_\mu}} \quad (2)$$

$$\varepsilon = \frac{u_*^3}{\kappa(z + z_0)} \quad (3)$$

where C_μ is a model constant (=0.09). The inlet specific turbulence kinetic energy, turbulence viscosity and turbulence intensity are subsequently given by:

$$\omega = \frac{\varepsilon}{C_\mu k} \tag{4}$$

$$v_t = \frac{k}{\omega} \tag{5}$$

$$I_u = \frac{\sqrt{\frac{2}{3}k}}{U(z)} \tag{6}$$

339

340 **Results**

341

342 *Field data*

343 Figures 4 and 5 display results for Case 1 (29 runs) and Case 2 (35 runs),
344 respectively. Areas of flow steering and reversal have been identified in parts A of
345 both figures and wind roses at each of the sensors are displayed in parts B and C.
346 The length of the arrows depends on the scatter of wind direction and the colour is a
347 function of the velocity ratio. Results confirm ideas by Walker and Nickling (2003)
348 and observations by Lynch *et al* (2010) at the same site, and show flow separation
349 and reversal on the lee-side of the foredune for offshore winds (Case 1) and flow
350 deflection for oblique winds (Case 2). The higher density array of this study has
351 allowed insights into the vertical behaviour of the flow. The wind direction for Case 1
352 and 2 remained constant at sensors deployed over the highest topographic point in
353 the profile (Figures 4A and 5A). Wind steering and/or flow reversal were measured at
354 the lowermost sensor in mast 2 and at heights below the foredune crest seaward for
355 both cases. This suggests the existence of permanent turbulent areas in the lee side
356 of the foredune under different angles of wind approach. Interestingly, the wind

direction presented an onshore component in sensors closer to the beach surface (mast 5–6) not only in Case 1 (as suggested by Lynch *et al.*, 2010) but also in Case 2. This has implications for potential onshore sediment transport (see discussion). Velocity ratios (*vr*) decreased closer to the ground (as expected) but surprisingly remained significantly constant independent of wind velocity at the reference sensor. Table 1 shows mean *vr* and corresponding standard deviations (σ) for each sensor. Note that the first row of data contains the maximum and minimum velocity found at the reference sensor to show the range of mean wind velocities for the 29 and 35 runs of Cases 1 and 2, respectively. Despite diversity in wind velocities at the reference sensor the standard deviations are very low, indicating small variability of individual *vr* with respect to the mean value given here. This is particularly useful in providing reasonable estimates of wind velocity at any of the sensors location given an incoming wind at the reference sensor but particularly at the unvegetated beach surface where sand grains may be entrained. Figure 6 displays regression curves between wind velocities at the reference sensor and sensors at 1 m high over the ground in masts 5 (dune toe) and 6 (back beach) for Case 1 (Figure 6A) and Case 2 (Figure 6B). Note that the maximum velocity attained during Case 1 winds was around 8 m s^{-1} while the maximum attained during Case 2 was 14.5 m s^{-1}. Despite a larger scatter in Case 2 there is a strong correlation in both sensors which could be useful in predicting wind velocity at 1 m over the beach surface given an incoming wind velocity (see Discussion).

Table 1. Mean velocity ratios (*vr*) and standard deviations (σ) obtained for each sensor using 29 10-min runs for Case 1 and 35 10-min runs for Case 2. Note that the range of wind velocities at the reference sensor is displayed in the first row

382

		Case 1		*Case 2*		
Array	Sensor height (m)	vr_1	σ_1	vr_2	σ_2	vr_1/vr_2
1	6 – reference sensor	max V = 8.03 m s^{-1}		max V = 14.45 m s^{-1}		
		min V = 2.35 m s^{-1}		min V = 3.16 m s^{-1}		
	1.5	0.86	0.02	0.82	0.01	1.1
2	16.3	0.95	0.03	0.97	0.04	1.0
	8	0.64	0.06	0.81	0.03	0.8
	1.5	0.35	0.03	0.48	0.02	0.7
3	6	0.97	0.04	0.92	0.05	1.1
	2	0.85	0.03	0.84	0.04	1.0
	1	0.75	0.04	0.80	0.04	0.9
4	6	0.88	0.04	0.84	0.05	1.0
	4	0.51	0.04	0.57	0.03	0.9
	2	0.25	0.02	0.41	0.02	0.6
	1	0.25	0.04	0.36	0.02	0.7
5	16.3	1.06	0.06	0.93	0.16	1.1
	11.9	0.98	0.05	0.87	0.07	1.1
	7.9	0.69	0.04	0.67	0.05	1.0
	4	0.30	0.03	0.45	0.04	0.7
	2	0.26	0.02	0.40	0.04	0.6
	1	0.25	0.02	0.30	0.03	0.8
6	16.2	0.99	0.06	0.92	0.07	1.1
	12.1	0.85	0.09	0.82	0.09	1.0
	8	0.55	0.05	0.65	0.06	0.8
	4	0.31	0.03	0.53	0.05	0.6
	2	0.28	0.03	0.49	0.05	0.6
	1	0.27	0.03	0.46	0.05	0.6

383

384 Finally, the comparison of *vr* in Table 1 indicates a stronger deceleration of the wind
385 in sensors below 4 m at masts 5 and 6 for Case 1, with wind velocities typically 60%
386 of the value of those in Case 2 most likely due to a higher degree of sheltering.
387 Figure 7 displays examples of wind profiles at each mast corresponding to the runs
388 with the highest mean velocities at the reference sensor for Case 1 (8 m s^{-1}) and
389 Case 2 (14.5 m s^{-1}). Only one run per case is presented because the pattern of wind
390 velocity across the dune was similar for a variety of input wind speeds. Wind velocity
391 decreased from mast 1 to mast 2 followed by a speed up close to original levels at
392 mast 3 (foredune crest). Wind velocities at the upper sections of the wind profiles in

masts 4 to 6 were comparable with velocities at the foredune crest, most likely indicating the free stream zone. As expected, velocities decreased closer to the surface, with the strongest vertical variation in wind velocity being recorded at mast 4, due to larger sheltering by the foredune.

CFD simulations

Figures 8 and 9 show results for LES-ABL and RANS k–ω SST simulations for Case 1 and 2 respectively. LES and IDDES simulations produced results that resemble those of RANS simulations and thus are not presented here. The turbulent models resolved the expected wind recirculation zone leeward of the foredune/beach interface for Case 1 (Figure 8, top images). The LES-ABL simulations predict lower near surface velocities compared with the RANS simulation, owing to the RANS model absence of wall roughness treatment and its inability to capture localized recirculation in depressions and valleys (between masts 1 and 3) along the rig line (Figure 8, bottom images). Both RANS and LES-ABL simulations suggest the recirculation zone reattachment point to be located at the beach surface downwind from the dune crest at approximately 4–5 times the foredune height. This is in line with observations by Frank and Kocurek (1996b) and Walker (2000) in aeolian dunes, and with observations by McLean and Smith (1986) and Nelson and Smith (1989) in fluvial dunes, with reattachment zones from 4–8 times the dune height. The 3-D simulations for Case 1 (bottom images) show no coherent terrain wind steering but instead predict localized recirculation zones along the beach/foredune system that are not two-dimensional.

LES-ABL simulations predicted smaller localized recirculation zones along the rig line for Case 2 (Figure 9, top images), including a small recirculation zone at the

418 foredune/beach location, isolated to the top of the dune. The Case 2 RANS
419 simulation did not predict any recirculation along the rig line. The dune system and
420 its alignment to the prevailing west winds are responsible for localized steering of the
421 wind toward the south-east as can be seen in Figure 5. Both the LES-ABL and
422 RANS simulations capture the near surface wind steering towards the south-east
423 (Figure 9, bottom images). However, the LES simulations predicted lower velocities
424 due to the inclusion of terrain roughness and their likely better resolution of near
425 surfaces eddies.
426
427 **Discussion**
428
429 *Comparison between measured and simulated CFD wind profiles*
430 Figures 10 and 11 show comparisons between velocity ratios measured in the field
431 and velocity ratios simulated by the four turbulent modelling approaches for Case 1
432 and Case 2, respectively. As expected, simulations performed without accounting for
433 terrain roughness (IDEES, LES, RANS) did not agree well with the measurements
434 and tended to over-predict the near-surface velocity. The results for the one-equation
435 LES-ABL simulations for Case 1 (Figure 10) agreed favourably with field
436 measurements for all six mast locations, including the recirculation zones captured
437 by masts 5 and 6 (Figure 4). Future simulations will be performed and compared
438 against this set using the IDDES with the terrain roughness modelling.
439 Figure 11 confirms that the LES-ABL simulations agree better with the measured
440 results compared with the simulations performed without aerodynamic roughness but
441 not at all sensors. While the introduction of a roughness parameter is important for
442 better agreement between LES-ABL simulations and field data, some of the wind

443 profiles in Figure 11 suggest room for further improvement. LES-ABL simulations in
444 Mast 3 and 1, for example, tend to under-estimate near-surface velocity, which may
445 be related to the way in which roughness is modelled. Velocity profiles in
446 Figure 7 suggest that the near surface wind velocities at these locations are less
447 dragged by roughness elements during oblique winds, which could result in an
448 under-estimation of LES-ABL simulations. Assumptions related to the use of the Law
449 of the Wall or a single value for roughness will therefore be explored in future work.
450 Typical values of $z_0 = 0.1$ m have been used elsewhere (Levin *et al.*, 2008) on a
451 similar terrain and alternative approaches to the calculation of z_0 have been
452 suggested by Levin *et al.* (2008) and Wakes *et al.* (2010).
453
454 *Geomorphological implications*
455 CFD 3-D simulations presented in Figure 8 (bottom images) indicate the
456 heterogeneity of surface airflow wind velocity and direction when emerging from the
457 foredune crest position. The modelling output shows alongshore patterns which
458 seem to be related to localized undulations in the foredune crest topography. On the
459 other hand, both 3-D simulations and field data indicate that airflow steering and
460 reversal are dependent on incident wind direction at the crest. The agreement
461 between simulated and observed velocity ratios at different heights across the
462 beach-dune profile and the output of 3-D simulations suggest several areas of future
463 research. first, field data needs to be acquired at a spatial grid over the beach
464 surface to validate CFD 3-D simulations. Second, and although previous research
465 has already observed landward sediment transport during offshore winds at this
466 location (Lynch *et al.*, 2008, 2009, 2010), there is a need to measure spatial
467 sediment transport patterns given the heterogeneity of wind velocity observed in 3-D

CFD simulations. Furthermore, there is a need to establish a relationship between potential onshore transport and wind velocity at a known location which could be used for predictive purposes. Although future work will deal with detailed transport dynamics, it is possible to speculate on the potential to perform simplified predictions of sediment input to the foredunes under offshore winds with the results presented here. According to Bagnold (1941), the threshold shear velocity for dry sand can be calculated as:

$$U_{*t} = A\left(\frac{\sigma-\rho}{\rho} g d\right)^{0.5} \quad (7)$$

where A is an empirical coefficient = 0.1 for air, σ is the density of grain material (2650 kg m^{-3} for quartz), d is the grain diameter (1.7 × 10^{-4} m), and ρ is the density of air (1.22 kg m^{-3}). This produces a U_{*t} = 0.19 m s^{-1} at Magilligan. Equation (1) can be applied to obtain a threshold velocity for dry sand movement (U_z) at any height z (assuming a logarithmic profile close to the surface). If the method of Namikas *et al.*(2003) is used, again with a wind profile obtained from sensors at heights 1 to 4 at mast 6 (bare sand) the roughness length z_0 = 10^{-3} m which in turn results in U_{1m} = 3.28 m s^{-1}. Correlations shown in Figure 6 (or velocity ratios displayed in Table 1) may then be used to find the minimum velocity at the reference sensor corresponding to U_{1m} = 3.28 m s^{-1} in mast 6. For example winds over 12.1 m s^{-1} (Case 1) and 7.1 m s^{-1} (Case 2) at the reference sensor would result in potential transport at the back beach. Wind direction at this location was steered landward and thus it is reasonable to expect onshore sediment movement (input to the foredune budget).

Finally, for ease of comparison, this paper has focused on 10 min averages of wind velocity. It is acknowledged that transport at the back beach is likely to be strongly influenced by turbulent structures and this will be the subject of future work. Shear stresses at the lee side of the dunes may be greater than those suggested by time-averaged streamwise estimates alone because of the role of turbulent stresses (Walmsley and Howard, 1985; Wiggs *et al.*, 1996). Shear stress generation, and thus the potential for sediment transport, is linked to turbulent fluctuations (i.e. flow unsteadiness) and the destabilizing effects of concave streamline curvature (Bradshaw, 1969; Wiggs *et al.*,1996; Walker and Nickling, 2003).

Conclusions

The present work describes the first results from field test measurements and comparative CFD simulations carried out to evaluate the off-shore wind flow over complex coastal dune terrain. LES simulations compare well with field measurements when an appropriate value for aerodynamic roughness is included in the model. The agreement obtained using the LES-ABL approach suggests that the CFD method can be used to examine the influences of topographic steering, which is an important element of aeolian sand transport at this and other sites. Furthermore, the LES-ABL results suggest that the method can help identify the recirculation zone location and the localized near-surface wind velocity and turbulence intensity. Such data can help identify the required windward wind characteristics needed to initiate sand transport either within a recirculation zone or along the upper beach during wind steering conditions. Future work will evaluate the performance of the IDDES simulation method with the ABL aerodynamic roughness treatment at the terrain boundary.

If the measured or simulated wind velocity ratios relevant to sand transport are combined with long-term meteorology records from a local reference station, a prediction of the frequency and intensity of foredune sand transport events may be possible. Further examination and comparison between CFD results and field tests is therefore important if sufficient confidence is to be placed in using CFD to simulate flow under other wind directions or different site and terrain conditions. Application of 3-D CFD over dune systems is, however, a valuable new tool that promises new insights into coastal dune geomorphology and dynamics. Finally, the approach may in fact be beneficial for other academic communities, such researchers interested in reconstructing past dune forming conditions for archaeological work or simulating foredune evolution under different climate change scenarios.

Acknowledgements

We wish to thank field technicians Robert Stewart, Sam Smyth and Peter Devlin for their unfaltering GPS field surveying efforts. Thanks are also extended to Colin Anderson (electronics workshop) and Nigel McCauley (mechanical workshop) whose expertise was paramount in the construction of the data interface system and instrument rig, respectively. Thomas Smyth provided invaluable assistance in the field. LIDAR information was used with the permission of Geological Survey, Ireland and access to the field site was kindly provided by Defence Estates, UK. This work is funded through the UK Natural Environment Research Council grant NE/F019483/1.

537

538 **References**

539 Abe K, Nagano Y, Kondoh T. 1993. Numerical simulations of separating and
540 reattaching flows with a modified low-Reynolds-number*k–e* model. *Journal of*
541 *Wind Engineering and Industrial Aerodynamics* 46–47: 85–94.

542 Anthony EJ, Vanhee S, Ruz M-H. 2007. Embryo dune development on a large,
543 actively accreting macrotidal beach: Calais, North Sea coast of France. *Earth*
544 *Surface Processes and Landforms* 32: 631–636.

545 Baas ACW, Sherman DJ. 2005. Formation and behavior of aeolian
546 streamers. *Journal of Geophysical Research Earth Surface* 110(F3): 15. DOI:
547 1029/2004JF000270.

548 Baddock MC, Livingstone I, Wiggs GFS. 2007. The geomorphological significance of
549 airflow patterns in transverse dune interdunes.*Geomorphology* 87: 322–336.

550 Bagnold RA. 1941. *The Physics of Blown Sand and Desert Dunes*. London:
551 Chapman and Hall.

552 Bauer BO, Davidson-Arnott RGD. 2003. A general framework for modelling sediment
553 supply to coastal dunes including wind angle, beach geometry and fetch
554 effects. *Geomorphology* 49: 89–108.

555 Bechmann A, Sørensen NN. 2010. Hybrid RANS/LES method for wind flow over
556 complex terrain. *Wind Energy* 13: 36–50.

557 Bradshaw P. 1969. The analogy between streamline curvature and buoyancy in
558 turbulent shear flow. *Journal of Fluid Mechanics*36:177–191.

559 Byrne CEI, Holdo AE. 1998. Effects of increased geometric complexity on the
560 comparison between computational and experimental simulations. *Journal of*
561 *Wind Engineering and Industrial Aerodynamics* 73: 159–179.

562 Castro I. 1991. Air flow and sand transport over sand dunes. *Acta*
563 *Mechanica* Supplement 2: 1–22.
564 Castro FA, Palma JMLM, Silva Lopes A. 2003. Simulations of the Askervein flow,
565 Part 1: Reynolds averaged Navier Stokes equations (k-ε turbulence
566 model). *Boundary-Layer Meteorology* 107: 501–530.
567 Delgado-Fernandez I, Davidson-Arnott RGD. 2010. Mesoscale aeolian sediment
568 input to coastal foredunes: the nature of aeolian transport
569 events. *Geomorphology* 126: 217–232.
570 DOI: 10.1016/j.geomorph.2010.11.005
571 Frank AJ, Kocurek G. 1996a. Toward a model for airflow on the lee side of aeolian
572 dunes. *Sedimentology* 43: 451– 458.
573 Frank AJ, Kocurek G. 1996b. Airflow up the stoss slope of sand dunes: limitations of
574 current understanding. *Geomorphology* 17:47–54.
575 Fröhlich J, Terzi D. 2008. Hybrid LES/RANS methods for the simulation of
576 turbulence flows. *Progress in Aerospace Sciences* 44:349–377.
577 Fryberger SG. 1979. Dune forms and wind regime. In *A Study of Global Sand*
578 *Seas*, McKeeED (ed). USGS Professional Paper 1052, US Geological Survey
579 and United States National Aeronautics and Space
580 Administration: Washington, DC; 137–169.
581 Gares PA, Nordstrom KF, Sherman DJ, Bauer BO, Davidson-Arnott RGD, Carter
582 RWG, Jackson D, Gomes N. 1993. Aeolian sediment transport under offshore
583 wind conditions: implications for aeolian sediment budget calculations.
584 In *Coastlines of Canada*,HildebrandLP (ed). American Society of Civil
585 Engineers: New York; 59–72.

586 Hesp PA. 2005. Topographic steering of offshore winds and dynamics of foredunes
587 and climbing dunes on a leeward east coast, New Zealand. In *Coasts Under*
588 *Stress II*, PsutyNP, ShermanDJ, Meyer-ArendtK (eds). Zeit. fur
589 Geomorphologie Supplement 141;123–134.
590 Illenberger WK, Rust IC. 1988. A sand budget for the Alexandria coastal dunefield,
591 South Africa. *Sedimentology* 35: 513–521.
592 Inkratas C, Gharabaghi B, Beltaos S, Krishnappan B. 2009. 3-D modelling of ice-
593 covered flows in the vicinity of a deep hole in the east channel of the
594 MacKenzie Delta, NWT. *Canadian Journal of Civil Engineering* 6(5): 791–800.
595 Jackson PS, Hunt JCR. 1975. Turbulent wind flow over a low hill. *Quarterly Journal*
596 *of the Royal Meteorological Society* 101: 929–955.
597 Jackson DWT, Cooper JAG, Del Rio L. 2005. Geological control on beach
598 state. *Marine Geology* 216: 297–314.
599 Kim HG, Patel VG. 2000. Test of turbulence models for wind flow over terrain with
600 separation and recirculation. *Boundary-Layer Meteorology* 94: 5–21.
601 Lane SN, Hardy RJ, Elliott L, Ingham DB. 2002. High-resolution numerical modelling
602 of three-dimensional flows over complex river bed topography. *Hydrological*
603 *Processes* 16: 2261–2272.
604 Lee SJ, Lim H-C, Park K-C. 2002. Wind flow over sinusoidal hilly obstacles located
605 in a uniform flow. *Wind and Structures* 5(6):515–526.
606 Levin N, Ben-Dor E, Kidron GJ, Yaakov Y. 2008. Estimation of surface roughness
607 (z_0) over a stabilizing coastal dune field based on vegetation and
608 topography. *Earth Surface Processes and Landforms* 33: 1520–1541.

609 Lun YF, Mochida A, Mutakami S, Yoshino H, Shirasawa T. 2003. Numerical
610 simulation of flow over topographic features by revised k-e models. *Journal of*
611 *Wind Engineering and Industrial Aerodynamics* 91: 231–245.
612 Lynch K, Jackson DWT, Cooper JAG. 2008. Aeolian fetch distance and topographic
613 steering: the influence of microscale variables on mesoscale foredune
614 development for leeside coasts. *Earth Surface Processes and*
615 *Landforms* 33: 901–1005.
616 Lynch K, Jackson DWT, Cooper JAG. 2009. Foredune accretion under offshore
617 winds. *Geomorphology* 105: 139–146.
618 Lynch K, Jackson DWT, Cooper JAG. 2010. Coastal foredune topography as a
619 control on secondary airflow regimes under offshore winds. *Earth Surface*
620 *Processes and Landforms*. 35: 344–353. DOI: 10.1002/esp.1925
621 McLean SR, Smith JD. 1986. A model for flow over two-dimensional bed
622 forms. *Journal of Hydraulic Engineering* 112: 300–317.
623 Menter FR. 1994. Two equation eddy-viscosity turbulence models for engineering
624 applications. *AIAA Journal* 32: 1598–1695.
625 Namikas SL, Bauer BO, Sherman DJ. 2003. Influence of averaging interval on shear
626 velocity estimates for aeolian transport modeling.*Geomorphology* 53: 235–
627 246.
628 Nelson J, Smith JD. 1989. Mechanics of flow over ripples and dunes. *Journal of*
629 *Geophysical Research* 94: 8146–8162.
630 Nguyen VT, Nestmann F. 2004. Applications of CFD in hydraulics and river
631 engineering. *International Journal of Computational Fluid*
632 *Dynamics* 18(2): 165–174.

633 Nicholas AP. 2001. Computational fluid dynamics modelling of boundary roughness
634 in gravel-bed rivers: an investigation of the effects of random variability in bed
635 elevation. *Earth Surface Processes and Landforms* 26: 345–362.
636 Nordstrom KF, Bauer BO, Davidson-Arnott RGD, Gares PA, Carter RWG, Jackson
637 DWT, Sherman DJ. 1996. Offshore aeolian transport across a beach: Carrick
638 Finn Strand, Ireland. *Journal of Coastal Research* 12(3): 664–672.
639 Nordstrom KF, Jackson NL, Klein AHF, Sherman DJ, Hesp PA. 2006. Offshore
640 aeolian transport across a low foredune on a developed barrier island. *Journal*
641 *of Coastal Research* 22(5): 1260–1267.
642 Parsons DR, Wiggs GFS, Walker IJ, Garvey BG, Ferguson RI. 2002. Time-averaged
643 numerical modeling of airflow over an idealized transverse dune.
644 In *Proceedings of ICAR5/GCTE-SEN Joint*
645 *Conference*, LeeJA, ZobeckTM (eds). International Center for Arid and
646 Semiarid Lands Studies, Publication 02–2, Texas Tech University: Lubbock,
647 Texas; 261.
648 Parsons DR, Walker IJ, Wiggs GFS. 2004. Numerical modelling of flow structures
649 over idealized transverse aeolian dunes of varying
650 geometry. *Geomorphology* 59: 149–164.
651 Raithby GD, Stubley GD, Taylor PA. 1987. The Askervein Hill project: a finite control
652 volume prediction of three-dimensional flows over the hill. *Boundary-Layer*
653 *Meteorology* 39: 247–267.
654 Richards PJ, Hoxey RP. 1993. Appropriate boundary conditions for computational
655 wind engineering models using the k-e turbulence model. *Journal of Wind*
656 *Engineering and Industrial Aerodynamics* 46/47: 145–153.

657 Safarzadeh AA, Neyshabouri S, Dehkordi AN. 2009. 2-D Numerical simulation of
658 fluvial hydrodynamics and bed morphological changes. In *Computational*
659 *Methods in Science and Engineering, Advances in Computational*
660 *Science*, SimosTE, MaroulisG (eds).American Institute of Physics Conference
661 Proceedings 1148, 2: 739–742.
662 Salmon JR, Bowen AJ, Hoff AM, Johnson R, Mickle RE, Taylor PA. 1988. The
663 Askervein hill experiment: mean wind variations at fixed heights above the
664 ground. *Boundary-Layer Meteorology* 43: 247–271.
665 Shennan I, Andrews J. 2000. Holocene land-ocean interaction and environmental
666 change around the North Sea. Geological Society Special Publications 166,
667 London.
668 Shi F, Huang N. 2010. Computational simulations of blown sand fluxes over the
669 surfaces of complex microtopography. *Environmental Modeling and*
670 *Software* 25(3): 362–367.
671 Shur ML, Spalart PR, Strelets MK, Travin AK. 2008. A hybrid RANS-LES approach
672 with delayed-DES and wall-modelled LES capabilities. *International Journal of*
673 *Heat and Fluid Flow* 29: 1638–1649.
674 Spalart PR. 2009. Detached-eddy simulation. *Annual Reviews of Fluid*
675 *Mechanics* 41: 181–202.
676 Spalart PR, Allmaras SR. 1994. A one-equation turbulence model for aerodynamic
677 flows. *Recherche Aerospatiale* 1: 5–21.
678 Spalart PR, Jou WH, Strelets MK, Allmaras SR. 1997. Comments on the feasibility of
679 LES for wings, and on a hybrid RANS/Les approach. In *Advances in*
680 *DNS//LES*, LiuC, LiuZ (eds). Greyden Press: Louisiana Tech
681 University. Ruston, LA, USA.

682 Spalart PR, Deck S, Shur ML, Squires KD, Strelets MK, Travin A. 2006. A new
683 version of the detached-eddy simulation, resistant to ambiguous grid
684 densities. *Theoretical Computational Fluid Dynamics* 20: 181–195.
685 Stangroom P. 2004. CFD modelling of wind flow over terrain. Unpublished PhD
686 thesis, University of Nottingham, UK.
687 van Boxel JH, Sterk G, Arens SM. 2004. Sonic anemometers in aeolian sediment
688 transport research. *Geomorphology* 59: 131.
689 Wakes SJ, Maegli T, Dickinson KD, Hilton MJ. 2010. Numerical modelling of wind
690 flow over a complex topography. *Environmental Modelling and*
691 *Software* 25: 237–247.
692 Walker IJ. 2000. Secondary airflow and sediment transport in the lee of transverse
693 dunes. PhD thesis, University of Guelph, Guelph.
694 Walker IJ. 2005. Physical and logistical considerations of using ultrasonic
695 anemometers in aeolian sediment transport research.*Geomorphology* 68: 57–
696 76.
697 Walker IJ, Nickling WG. 2002. Dynamics of secondary airflow and sediment
698 transport over and in the lee of transverse dunes.*Progress in Physical*
699 *Geography* 26(1): 47–75.
700 Walker IJ, Nickling WG. 2003. Simulation and measurement of surface shear stress
701 over isolated and closely spaced transverse dunes. *Earth Surface Processes*
702 *and Landforms* 28: 1111–1124.
703 Walker IJ, Hesp PA, Davidson-Arnott R, Ollerhead J. 2006. Topographic steering of
704 alongshore airflow over a vegetated foredune: Greenwich Dunes, Prince
705 Edward Island, Canada. *Journal of Coastal Research* 22(5): 1278–1291.

706 Walmsley JL, Howard AD. 1985. Application of a boundary-layer model to flow over
707 an aeolian dune. *Journal of Geophysical Research* 90(D6): 10631–10640.
708 Wiggs GFS, Livingstone I, Warren A. 1996. The role of streamline curvature in sand
709 dune dynamics: evidence from field and wind tunnel
710 measurements. *Geomorphology* 17: 29–46.

711

712 List of figures

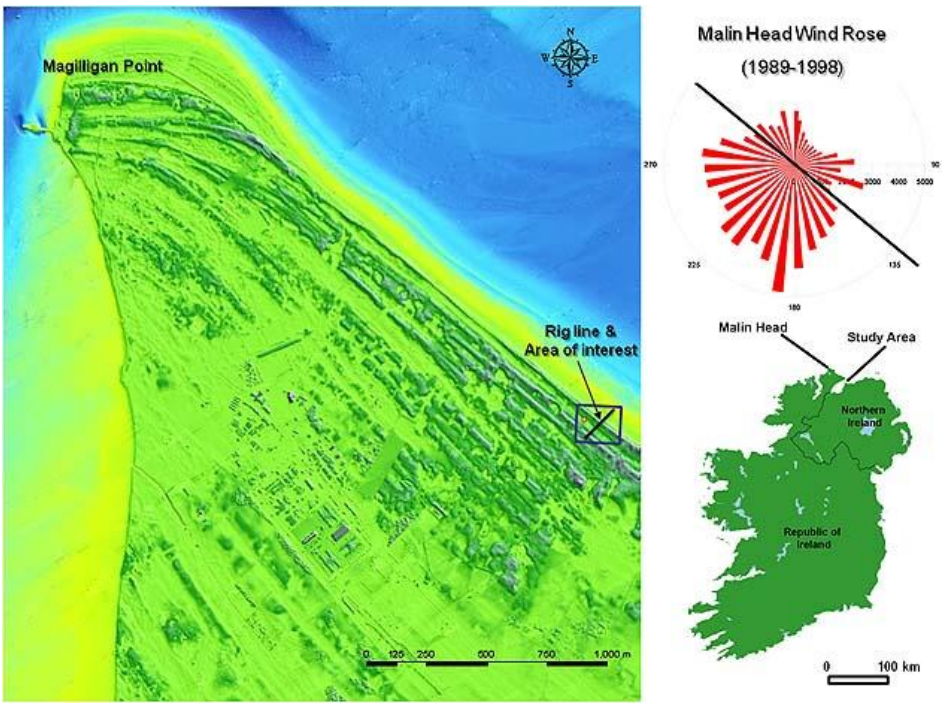

Figure 1. Location of rig line at Magilligan point, Northern Ireland. The wind rose displays the distribution of regional wind speed and direction at Malin Head.

713

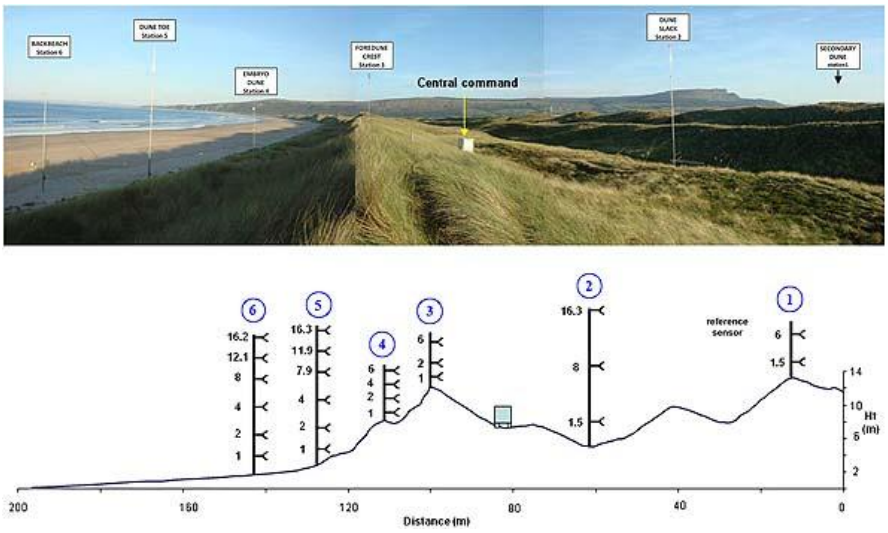

Figure 2. Location of the six vertical arrays (masts) containing 24 three-dimensional ultrasonic anemometers along the dune cross-section. Instrument elevations ranged from 1 m to 16.3 m over the beach–dune surface. Vegetation was present at masts 1 to 4 and consisted of marram grass of approximately 0.35 m height. The different zones of the beach–dune system (from the secondary dune to the back beach) are identified for each of the masts, as well as the position of the reference sensor (6 m height at mast 1).

714

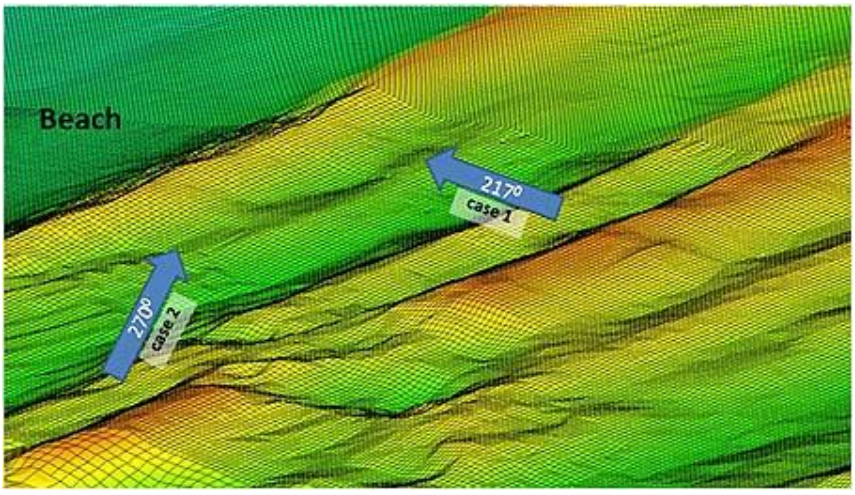

Figure 3. Detailed topographic mesh surface from the merger of LIDAR and DGPS data. Case 1 contained perpendicular offshore winds and Case 2 contained oblique

offshore winds (217° and 270°, respectively, at Magilligan).

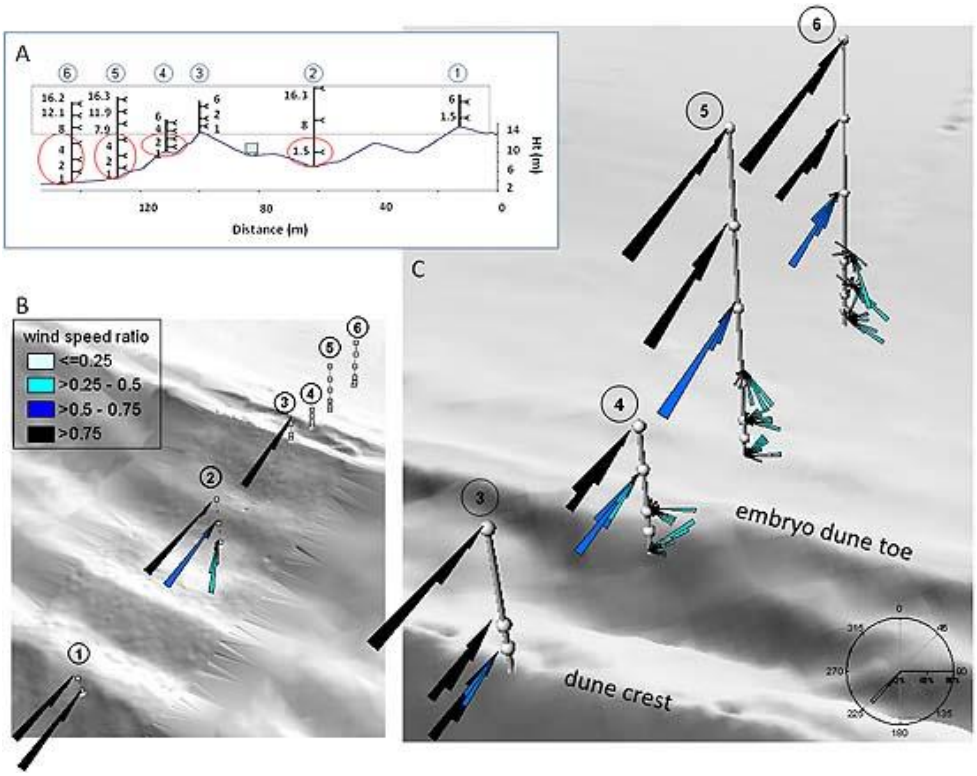

Figure 4. Field results for Case 1. (A) Steering and flow reversal zones across the dune profile (circled red) where below the maximum topographic height, and zones of constant wind direction above it (boxed area); (B) wind roses in masts 1 to 3 (at 6 m high); (C) wind roses at masts 3 to 6. Wind direction has been binned every 5° and wind velocity is expressed as the velocity ratio.

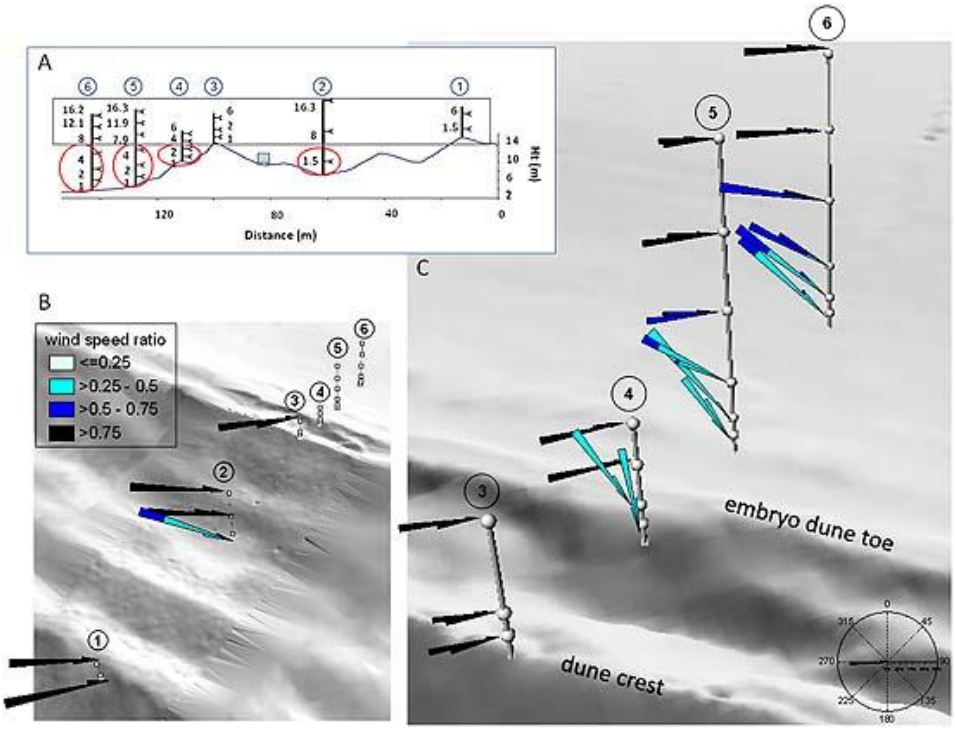

Figure 5. Field results for Case 2. (A) Steering and flow reversal zones across the dune profile (circled red) where below the maximum topographic height, and zones of constant wind direction above it (boxed area); (B) wind roses in masts 1 to 3 (at 6 m high); (C) wind roses at masts 3 to 6. Wind direction has been binned every 5° and wind velocity is expressed as the velocity ratio.

717

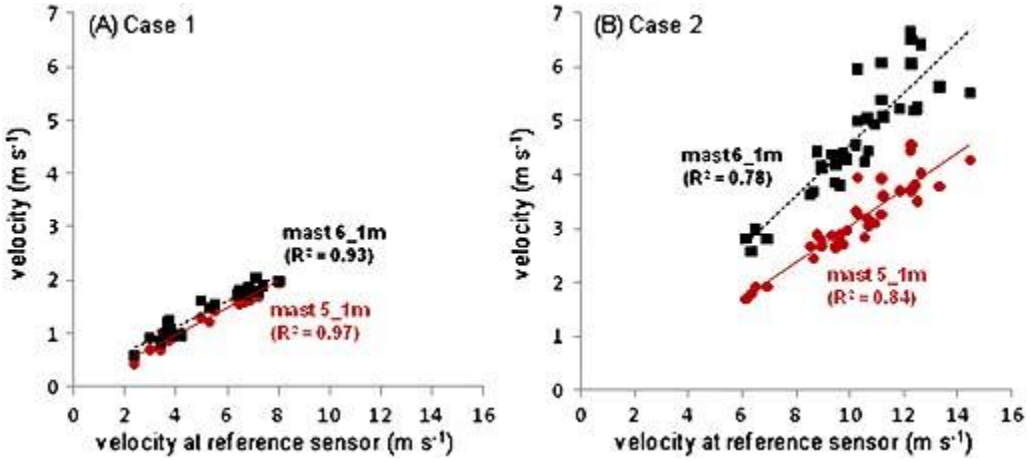

Figure 6. Regression curves between wind speed measured at the reference sensor and wind speed measured at 1 m height over the beach surface at masts 5 and 6 for

Case 1 (A) and Case 2 (B).

718

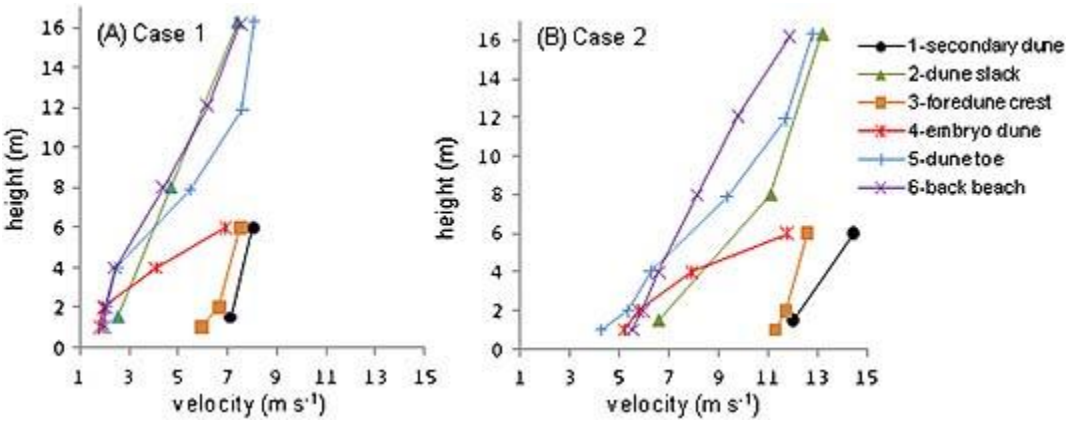

Figure 7. Examples of velocity profiles for Case 1 (A) and Case 2 (B).

719

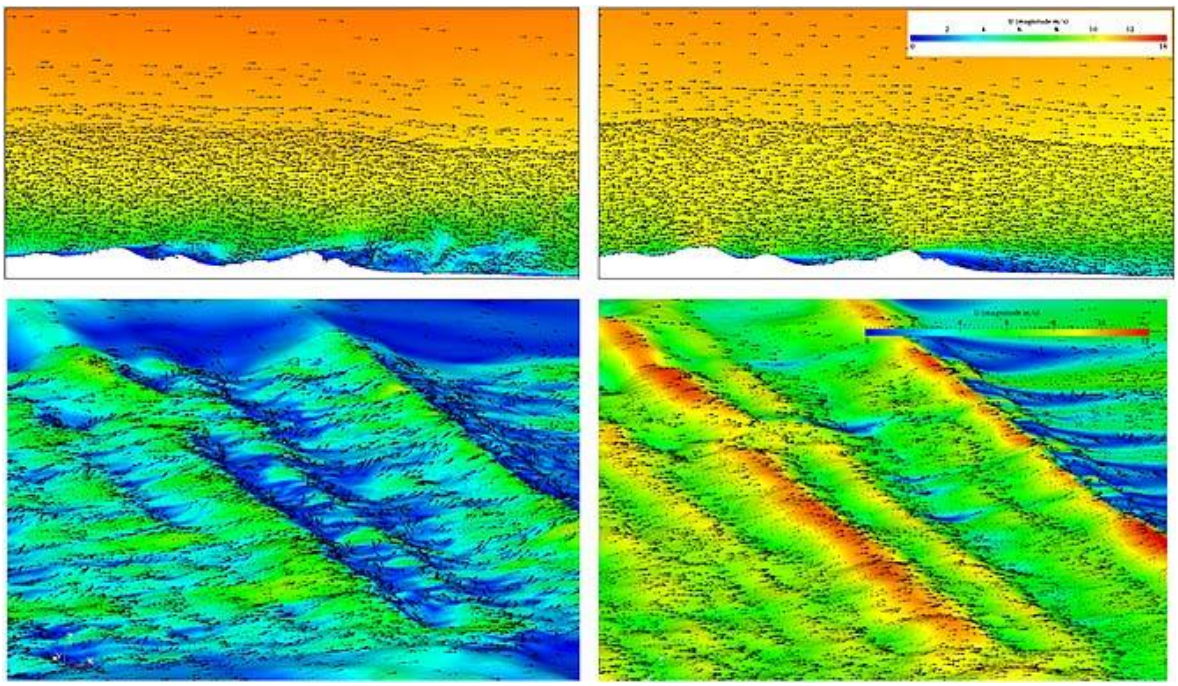

Figure 8. Case 1 velocity vectors and contours for a vertical plane through the rig line (top) and at 2 m above the terrain (bottom). Left images: LES-ABL; Right images: RANS k-ω SST.

720

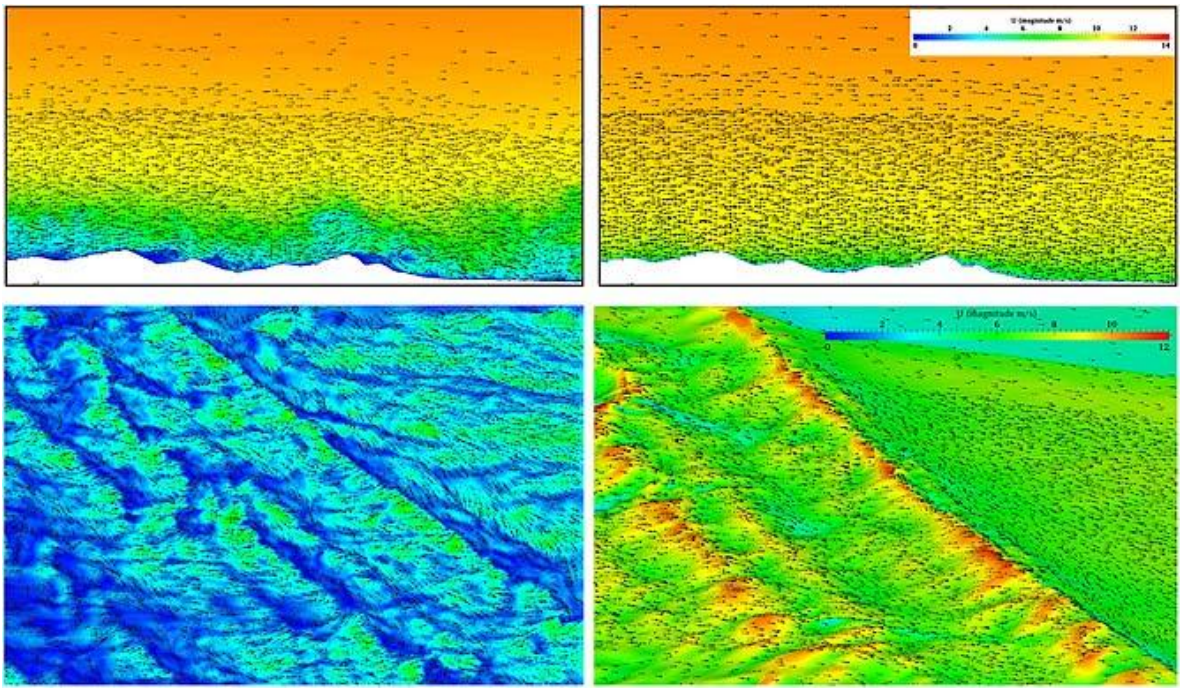

Figure 9. Case 2 velocity vectors and contours for a vertical plane through the rake line (top) and at 2 m above the terrain (bottom). Left images: LES – ABL; Right images: RANS k-ω SST.

721

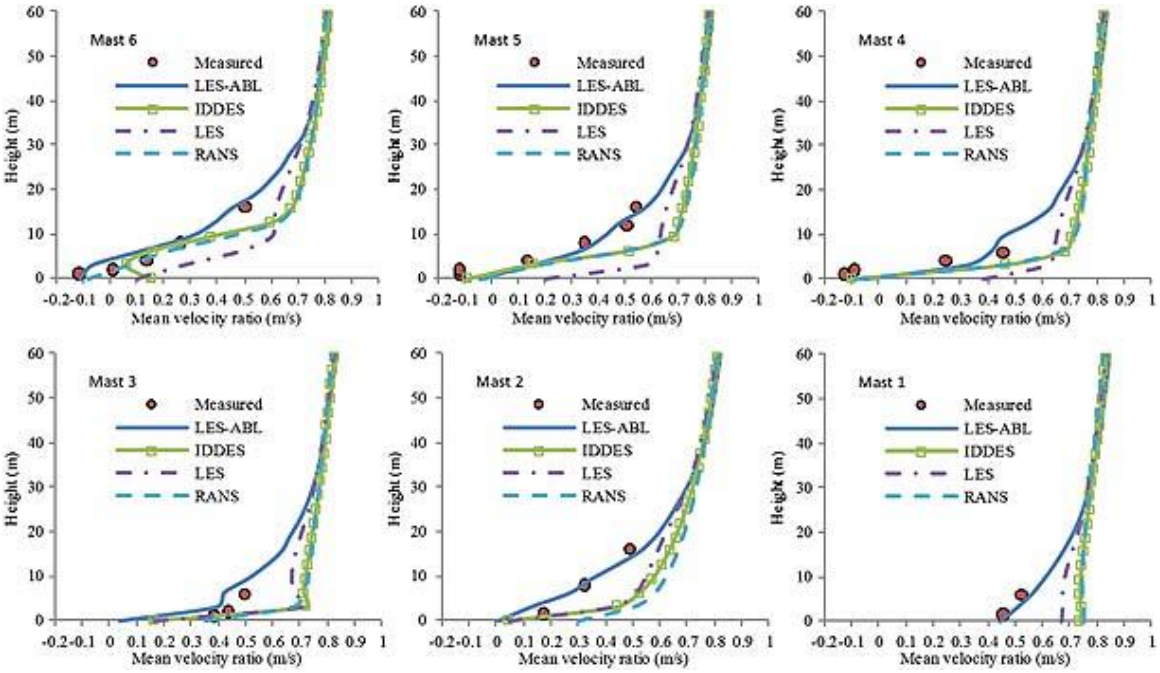

Figure 10. Comparison between Case 1 measured and CFD mean velocity ratios

(Masts 1–6).

722

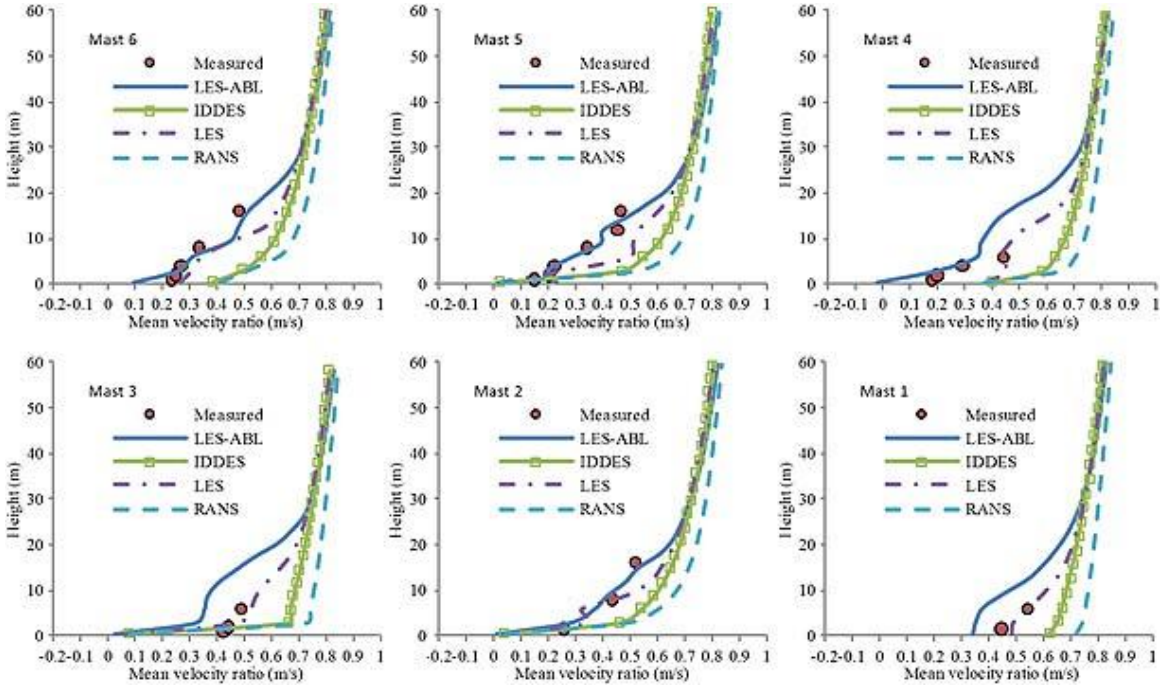

Figure 11. Comparison between Case 2 measured and CFD mean velocity ratios (Masts 1–6).

723